Proc. Natl. Acad. Sci. USA
Vol. 92, pp. 3869–3873, April 1995
Biophysics

Bacteriophage T7 helicase/primase proteins form rings around single-stranded DNA that suggest a general structure for hexameric helicases

(DNA helicase/three-dimensional reconstruction/DNA replication)

EDWARD H. EGELMAN*†, XIONG YU*, ROBERT WILD*, MANJU M. HINGORANI‡, AND SMITA S. PATEL‡

*Department of Cell Biology and Neuroanatomy, University of Minnesota Medical School, Minneapolis, MN 55455; and ‡Department of Biochemistry, The Ohio State University, 484 West 12th Avenue, Columbus, OH 43210

Communicated by F. William Studier, Brookhaven National Laboratory, Upton, NY, January 17, 1995

ABSTRACT **Most helicases studied to date have been characterized as oligomeric, but the relation between their structure and function has not been understood. The bacteriophage T7 gene *4* helicase/primase proteins act in T7 DNA replication. We have used electron microscopy, three-dimensional reconstruction, and protein crosslinking to demonstrate that both proteins form hexameric rings around single-stranded DNA. Each subunit has two lobes, so the hexamer appears to be two-tiered, with a small ring stacked on a large ring. The single-stranded DNA passes through the central hole of the hexamer, and the data exclude substantial wrapping of the DNA about or within the protein ring. Further, the hexamer binds DNA with a defined polarity as the smaller ring of the hexamer points toward the 5′ end of the DNA. The similarity in three-dimensional structure of the T7 gene *4* proteins to that of the *Escherichia coli* RuvB helicase suggests that polar rings assembled around DNA may be a general feature of numerous hexameric helicases involved in DNA replication, transcription, recombination, and repair.**

DNA helicases are ubiquitous proteins that unwind double-stranded DNA (dsDNA) into single-stranded DNA (ssDNA), using energy from NTP hydrolysis (1). Interestingly, most of the helicases that have been studied to date self-assemble into either dimers or hexamers (2, 3). The significance of oligomerization in helicases is unclear, as the mechanism of DNA unwinding is not understood. Bacteriophage T7 gene *4* proteins provide the helicase and primase functions for T7 DNA replication and both proteins have been shown to form stable hexamers in the presence of Mg^{2+} and thymidine 5′-[β,γ-methylene]triphosphate (dTTP[β,γ-CH_2]), a nonhydrolyzable analog of dTTP (4). All data suggest that the hexamer is the active form of the protein involved in DNA unwinding, since hexamer formation is required for DNA binding, and substitution of a few of the hexameric subunits with inactive subunits inhibits both the DNA-dependent dTTPase and the helicase activities of the protein (5). We report here the structures of T7 gene *4A′* and *4B* proteins and their mode of DNA binding, using the techniques of electron microscopy, three-dimensional reconstruction, and protein crosslinking.

MATERIALS AND METHODS

Preparation of Gene *4* Protein–DNA Complexes. T7 gene *4A′* and *4B* proteins were prepared as described (6). Preparations in the absence of DNA involved incubations of the protein (0.7 μM) for 10 min at 37°C in 25 mM triethanolamine buffer (pH 7.2) with 2 mM magnesium acetate and 1.3 mM dTTP[β,γ-CH_2]. Preparations with ssDNA were similar, except that the protein concentration was 1.5 μM and the DNA concentration was 0.6 nM.

Synthesis of α-^{32}P-Labeled-ssDNA. Radiolabeled linear ssDNA was prepared by elongating a 30-mer oligodeoxynucleotide with terminal deoxynucleotidyltransferase. The reaction mixture contained 0.7 μM 30-mer, 0.5 mM each dNTP, [α-^{32}P]dTTP [20 μCi (740 kBq)], 1 mM $CoCl_2$, and 35 units of terminal deoxynucleotidyltransferase (Boehringer Mannheim), 200 mM potassium cacodylate, 25 mM Tris·HCl, and 0.025% bovine serum albumin at pH 6.6. The mixture was incubated for 2 hr at 37°C, and the unincorporated dNTPs were removed by gel filtration. The average length of uniformly radiolabeled ssDNA was estimated from the molar amount of dNTPs incorporated and was found to be around 200 nt.

Electron Microscopy. Specimens were applied to glow-discharged grids, stained with 2% (wt/vol) uranyl acetate, and imaged under minimal dose conditions in a JEOL 1200 EXII electron microscope, at a nominal magnification of ×30,000.

Image Analysis. A reference-free algorithm (7) was used for determining the translations and rotations needed to bring individual images of the gene *4* protein complexes into a common alignment, after floating of the images to zero-mean density, contrast normalization, and band-pass filtration. A filtered back-projection algorithm was used for the three-dimensional reconstruction. These procedures were implemented with SPIDER software package (8). A neural-net classification algorithm (9, 10) was used to decompose the averages into characteristic views.

RESULTS

The 63-kDa 4A′ helicase/primase protein is a $Met^{64} \rightarrow Leu$ mutant of 4A that has wild-type helicase and primase activities (6). The Met^{64} codon is the initiation codon for the 4B protein and has been mutated to express 4A′ alone. The 56-kDa 4B protein, which is translated from an internal initiation site in 4A, lacks the N-terminal 63 aa and has only helicase activity (11). Fig. 1 *a* and *d* show "top view" images of 4A′ and 4B proteins, respectively, assembled in the presence of Mg^{2+}-dTTP[β,γ-CH_2] but in the absence of DNA. Images in the electron microscope suffer from a very poor signal/noise ratio; thus averaging of images was used to reliably see structural detail. From fields of assemblies such as those shown in Fig. 1 *a* and *d*, 1000 images of the 4A′ rings and 800 images of the 4B rings were selected. The averaged images (Fig. 1 *b* and *e*) of 4A′ and 4B proteins are quite similar and show six subunits of the proteins arranged in a ring with a distinct hole in the middle. The diameter of the ring is ≈130 Å and the diameter of the

The publication costs of this article were defrayed in part by page charge payment. This article must therefore be hereby marked "*advertisement*" in accordance with 18 U.S.C. §1734 solely to indicate this fact.

Abbreviations: dsDNA, double-stranded DNA; ssDNA, single-stranded DNA; dTTP[β,γ-CH_2], thymidine 5′-[β,γ-methylene]triphosphate.

†To whom reprint requests should be addressed.

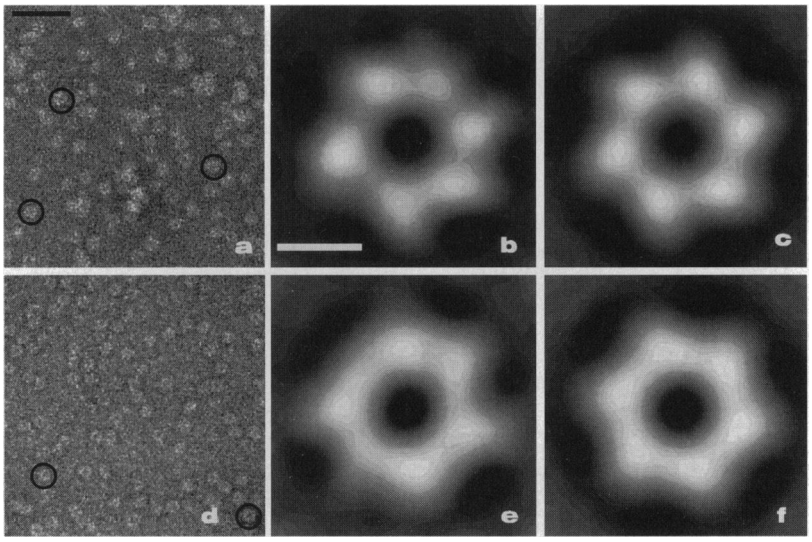

FIG. 1. (*Left*) Electron micrographs of T7 4A′ protein (*a*) and 4B protein (*d*), prepared in the absence of DNA but with the nonhydrolyzable dTTP analog dTTP[β,γ-CH_2]. (Bar in *a* = 500 Å.) Images of individual rings were masked off from their surroundings, as shown by the circles in *a* and *d* and were aligned and averaged by a reference-free algorithm (7). (*Center*) Averages of such top-view images are shown for 4A′ (1000 images) and 4B (800 images) (*b* and *e*, respectively). (Bar in *b* = 50 Å.) No symmetry has been imposed during the averaging process, but the final averages have a strong sixfold rotational power, with no significant twofold or threefold power (data not shown) that might arise from a dimer of trimers or a trimer of dimers. (*Right*) An exact sixfold symmetry has been imposed upon the averages in *b* and *e*, generating the images in *c* and *f*, respectively. The ring is about 130 Å in diameter, with a strongly stained hole in the center that is 25–30 Å in diameter.

hole is 25–30 Å. The ring-like arrangement of the hexamer suggests that the interaction between subunits is only between nearest neighbors. The deviations that exist in the averages from perfect sixfold symmetry are presumably due to noise, since there is no significant twofold or threefold rotational component that might arise from a dimer of trimers or a trimer of dimers. We have therefore imposed a sixfold symmetry on the averages, as shown in Fig. 1 *c* and *f*. A slight "handedness" can be seen in the 4A′ protein average, suggesting that these rings may lie with a preferred orientation on the carbon substrate, since a random distribution of orientations would cancel any handedness in the average. The absence of this handedness in the 4B average (Fig. 1*f*) suggests that this feature arises from either the additional 63 aa present at the N terminus of 4A′ or a conformational difference. Attempts to decompose each of the averages into subsets based upon similarity, using both multivariate statistical analysis (12) and a neural-net learning algorithm (9, 10), did not reveal any subsets that showed a stronger handedness or any other interesting deviation from the total averages.

When the gene *4* proteins were assembled on M13mp8 ssDNA in the presence of Mg^{2+}-dTTP[β,γ-CH_2], stacked ring-like structures could be seen on the DNA (Fig. 2 *a* and *c*). We can show (see below) that these images of the protein on the DNA correspond to "side views" of the rings shown in Fig. 1 in the absence of DNA. On DNA molecules that appear nearly fully covered by protein, ≈250 4B rings can be counted per circle, which corresponds to an ≈90-Å separation between adjacent rings. This characteristic spacing can also be seen by using Fourier analysis of straight, rod-like regions. The 4A′ protein, however, has a much greater variability in the spacing between rings. The closest packing corresponds to an ≈96-Å separation, and regularly spaced separations as large as 102 Å can be seen for the 4A′ rings. This suggests that the additional 63 aa at the N terminus of 4A′ may be located near the ends of the rings when one looks along the DNA. Image analysis failed to reveal any rotational alignment between adjacent rings, suggesting that the rings may be rotationally oriented in a random or nearly random manner with respect to nearest neighbors.

For single-particle image analysis, one needs to cut out images of isolated particles from a field, without any overlap of density from surrounding particles. Because the rings of both the 4A′ and the 4B protein are packed so closely together, this was virtually impossible to accomplish with the poor signal/noise ratio in the raw images. Use of lower protein concentrations with the same concentration of the DNA did not lead to more separated rings, indicating that there is a cooperativity in protein binding to the DNA. Given the lack of defined relationship between the rings, it should be noted that this cooperativity does not necessarily result from a ring–ring interaction but may result from the relaxation of ssDNA secondary structure by one ring leading to further ring formation in the same area. We have therefore cut out groups of three rings for averaging, using an averaging procedure that will attempt to align only the central ring of the three rings.

The averages from 1000 images of the 4A′ rings (Fig. 2*b*) and 1000 images of the 4B rings (Fig. 2*d*) show that each hexamer appears two-tiered with a small ring stacked on a large ring. The average from the 4B rings is much sharper, suggesting that the rings are aligned uniformly in a perpendicular orientation with respect to the top view, possibly due to their close packing. The 4A′ rings, on the other hand, may have a random rotational component both about the axis of the DNA and about an axis perpendicular to the DNA. The averaging procedure used ignores the surrounding two rings and forces the alignment to be on the center ring. Therefore, the surrounding two rings in the 4B protein average (Fig. 2*d*) can be seen as "blurred" versions of the central ring, with a lower contrast. The surrounding two rings in the average, however, show that adjacent 4B protein rings are oriented along the DNA with the same polarity. A similar analysis for 4A′ rings, using a larger averaging window, demonstrated a similar result (data not shown). If the structures on the DNA correspond to side views of the rings formed in the absence of DNA (Fig. 1), then the projection of the averaged side views (which are cylindrically averaged due to their random orientations) onto a line perpendicular to the DNA axis should be the same as the projection of the cylindrically averaged top view onto a line passing through the center of the ring. This has been done and the projections are in excellent agreement (data not shown),

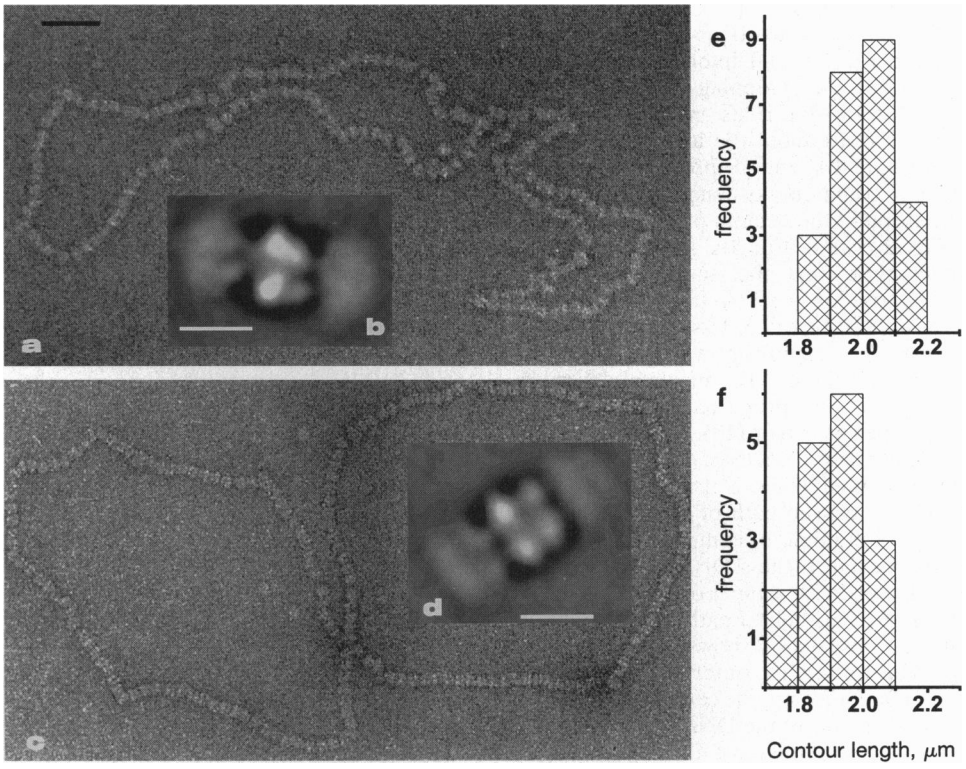

FIG. 2. Electron micrographs of M13mp8 ssDNA circles covered with 4A′ protein rings or 4B rings are shown in *a* and *c*, respectively. (Bar in *a* = 500 Å.) Groups of three adjacent rings were masked off from their surroundings and were aligned and averaged (7). The average of 4A′ protein is shown in *b*, and the 4B average in *d*. (Bars in *b* and *d* = 100 Å.) The alignment procedure imposed an outer diameter limit of 144 Å on the rotational search, and as a result of this the central structure of the group of three is well aligned, while the two surrounding units are blurred due to variability in spacing of the rings and curvature of the DNA. The structures are about 130 Å in diameter, and data analysis shows that these projections are consistent with being side-views of the rings formed in the absence of DNA, shown in Fig. 1. The contour lengths of 24 4A′-covered M13mp8 ssDNA circles (*e*) and 16 4B-covered M13mp8 ssDNA circles (*f*) were measured. The maximum extension observed precludes any significant wrapping of the DNA within or about the rings.

supporting the notion that the two types of averages correspond to orthogonal projections of the same structure.

Most helicases function *in vitro* with a defined polarity with respect to a ssDNA substrate on which a complementary second strand has been annealed. The gene *4* proteins are believed to translocate and unwind DNA in the 5′-to-3′ direction (13, 14). As the hexamers bind DNA with a defined polarity, the following experiment was performed to determine the structural polarity of the rings with respect to the DNA polarity. Linear dsDNA molecules were partially digested with exonuclease III, creating 5′ ssDNA tails on both ends of linear dsDNA (15), and these substrates were incubated with 4B protein. As expected, the hexamers bound only to the ssDNA regions (Fig. 3), and image analysis showed that the small rings of the hexamer all pointed toward the 5′ end of the ssDNA to which the rings were bound. It is not clear how the hexamer interacts with the forked DNA substrate that it unwinds. However, if the hexamer binds to the 5′ ssDNA tail of a forked DNA, then these results show that the gene *4* protein hexamer would move on the DNA with the large ring facing the dsDNA region being unwound. The defined orientation of the hexamer on the DNA must be related to the unidirectional translocation observed for the gene *4* proteins on ssDNA (13).

Previous nuclease-protection experiments have shown that both 4A′ and 4B hexamers protect about 25–30 nt of ssDNA (16). This is in agreement also with the finding that the 7229 bases of M13mp8 DNA are completely covered by about 250 hexameric rings of 4B protein. Hence, each hexameric ring covers about 29 bases of ssDNA. Protein–DNA crosslinking experiments have shown that a 30-mer ssDNA interacts with or is in proximity to at least five and perhaps all six subunits of the hexamer (5). These results exclude wrapping of the DNA on the outside of the ring as suggested for RNA binding to the

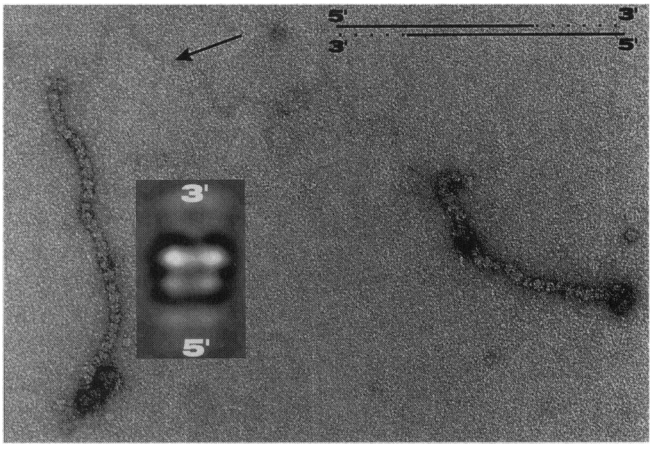

FIG. 3. Polarity of the 4B rings with respect to ssDNA. ϕX174 dsDNA was linearized with restriction endonuclease *Ssp* I (Promega) and then digested with exonuclease III (Promega) for 3 min at 37°C as described (15). Since exonuclease III processively digests the 3′ ends of the dsDNA, DNA substrates are created with single-stranded 5′ tails, as shown in the schematic diagram at top right. These DNA molecules were incubated with 4B protein, forming structures such as that shown containing two 4B-covered tails with a naked dsDNA region in between (arrow). The polarity of the 4B rings was determined by translationally averaging rings along the ssDNA, and the *Inset* shows that the smaller, less dense part of the ring is at the 5′ end. The *Inset* is an average of 800 4B rings aligned by using a 120-Å limit on the diameter of the rotational search.

hexameric *Escherichia coli* Rho protein (17), because it is not possible for a 30-nt DNA to stretch to about 14 Å per base to wrap around the outer periphery and interact with all the subunits of the ring. Further, any wrapping of the DNA, or binding of DNA to the sides of the rings, most likely would introduce a stagger of the rings about the axis of the DNA. Instead, what is seen for both 4A′ and 4B proteins is that the rings are aligned along a common axis, suggesting that the DNA must be passing through the centers of these rings.

Contour lengths (Fig. 2 *e* and *f*) of 4A′ and 4B protein-covered ssDNA circles show that the maximal extension corresponds to an axial rise of ≈3.0 Å per base. This is consistent with the DNA passing more or less directly through the center of each ring. Any significant wrapping can be excluded by the following calculation. The maximal observed extension of DNA occurs in the presence of intercalating agents and is about 6.8 Å per base pair (18). If one takes this as the maximal axial rise per base in ssDNA, then the 29 bases associated with each ring might have a maximum contour length of about 200 Å. Any curved path of the DNA would need to contain an integral multiple of complete turns, so as to allow the rings to be coaxial. If the ssDNA made a single helical turn around each ring, with a pitch of 90 Å, then the maximum possible radius for this helical path would be 28 Å. As a three-dimensional reconstruction shows (below), such a path does not seem possible around the outer periphery of the structure. While a helical path through the central hole cannot be excluded, the sixfold symmetry of the DNA-binding sites is inconsistent with such a path, and the most likely possibility is that the DNA is binding one subunit of each hexamer while traveling along or near the axis of the rings.

Additional data showing that the ssDNA passes through the hole of the hexameric ring comes from an experiment in which 4A′ hexamers were assembled on circular M13 ssDNA in the presence of Mg^{2+}-dTTP[β,γ-CH_2], and the subunits were then chemically crosslinked with a bifunctional crosslinking reagent. If 4A′ hexamers assemble around the DNA, then crosslinked hexamers will get trapped on circular M13 DNA and will not dissociate from the DNA even under denaturing conditions. On the other hand, if the DNA does not pass through the hole, then crosslinked hexamers will dissociate from the DNA under denaturing conditions. The electrophoretic mobility of M13 ssDNA shifted when the DNA was complexed to increasing amounts of 4A′ protein (Fig. 4*a*, lanes 1–4) and analyzed in a nondenaturing agarose gel. The same shift was observed with the crosslinked 4A′ protein (lanes 6–8). When the samples were heat-denatured in the presence of SDS and electrophoresed in an SDS-containing agarose gel (Fig. 4*b*), the uncrosslinked protein dissociated from the DNA, as expected, but the crosslinked protein remained bound to the DNA, showing that the DNA was bound to the hexameric ring through the hole. Control crosslinking experiments with linear ssDNA showed that the trapping was not due to covalent crosslinking of the DNA to the protein, as crosslinked hexamers dissociated from linear ssDNA during electrophoresis (Fig. 4 *c* and *d*).

A three-dimensional reconstruction of the 4B protein ring was determined (Fig. 5) by employing both the hexameric symmetry and a classification into characteristic views, to generate the equivalent of projections obtained from a single-axis tilt series about the axis of the DNA. Each of the six subunits in the ring must contain two lobes or domains, with one lobe forming the large ring and the other forming the small ring. The findings that the subunits of the hexameric helicase are arranged in a ring and that the ssDNA interacts within the hole provide important insights into the mechanism of this helicase. One mechanism by which the hexamer may translocate on ssDNA is by interaction of consecutive subunits of the ring with the DNA. Such a scheme could explain why the introduction of only a few inactive subunits into each hexamer

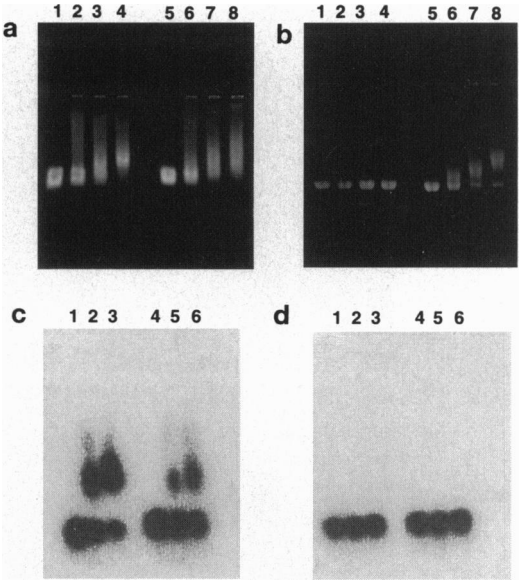

FIG. 4. Crosslinked 4A′ hexamers bound to M13 ssDNA. (*a*) 4A′ protein was assembled on M13 ssDNA (0.07 μM) in the presence of Mg^{2+}-dTTP[β,γ-CH_2] (200 μM) and either incubated at 22°C or crosslinked with dimethyl suberimidate (10 mg/ml) for 12 min at 22°C. The samples were quenched with glycine (1 M) and subsequently electrophoresed in a nondenaturing 1% agarose gel containing 10 mM magnesium acetate and 80 μM dTTP[β,γ-CH_2]. Lanes 1 and 5, free M13 DNA; lanes 2–4 and 6–8, M13 ssDNA bound to 5, 15, and 30 μM uncrosslinked and crosslinked 4A′ protein, respectively. (*b*) The same samples as in *a* were heat-denatured at 90°C in the presence of 1% SDS and electrophoresed in a 1% agarose gel containing 0.1% SDS. (*c*) Samples were electrophoresed in a nondenaturing 1% agarose gel containing Mg^{2+}-dTTP[β,γ-CH_2]. Lanes 1 and 4, free uniformly radiolabeled linear ssDNA; lanes 2 and 3 and lanes 5 and 6, ssDNA bound to 15 and 30 μM uncrosslinked and crosslinked 4A′ protein, respectively. (*d*) The same samples as in *c* were heat-denatured at 90°C in the presence of SDS and electrophoresed in a 1% agarose gel containing 0.1% SDS.

can greatly decrease the helicase and NTPase activities of the protein (5, 20). Conformational changes facilitated by the NTPase reaction may allow the subunits to bind and dissociate from the DNA during translocation, as NTP binding promotes DNA binding and NTP hydrolysis may lead to DNA dissociation (16). The binding of the DNA within the hole of stable hexamers is the basis for the high processivity of translocation that was observed with the gene *4* proteins on ssDNA (13).

DISCUSSION

The three-dimensional reconstruction of the 4B hexamer is striking in its similarity to half of the *E. coli* RuvB dodecamer (19), where the RuvB dodecamer consists of two hexameric rings that are oriented in a bipolar manner on dsDNA. RuvB is the product of a DNA damage-inducible gene, and it is involved in the branch migration of Holliday junctions that occur during homologous recombination (21). RuvB also shares the characteristic helicase sequence motifs with the T7 gene *4* proteins (22), and interestingly, both proteins appear to unwind DNA in the 5′-to-3′ direction (14, 23). The similarity of the 4B and RuvB reconstructions suggests that structural conservation may be much stronger than the limited sequence conservation among certain helicase proteins. While data suggest that some helicases function as dimers, numerous other helicases appear to be organized as hexamers (2, 3, 24, 25). The simian virus 40 large tumor (T)-antigen helicase protein exists as both single and double hexameric rings (26), and both structural species are functionally active (27). It has been proposed that the T-antigen hexameric rings form around the

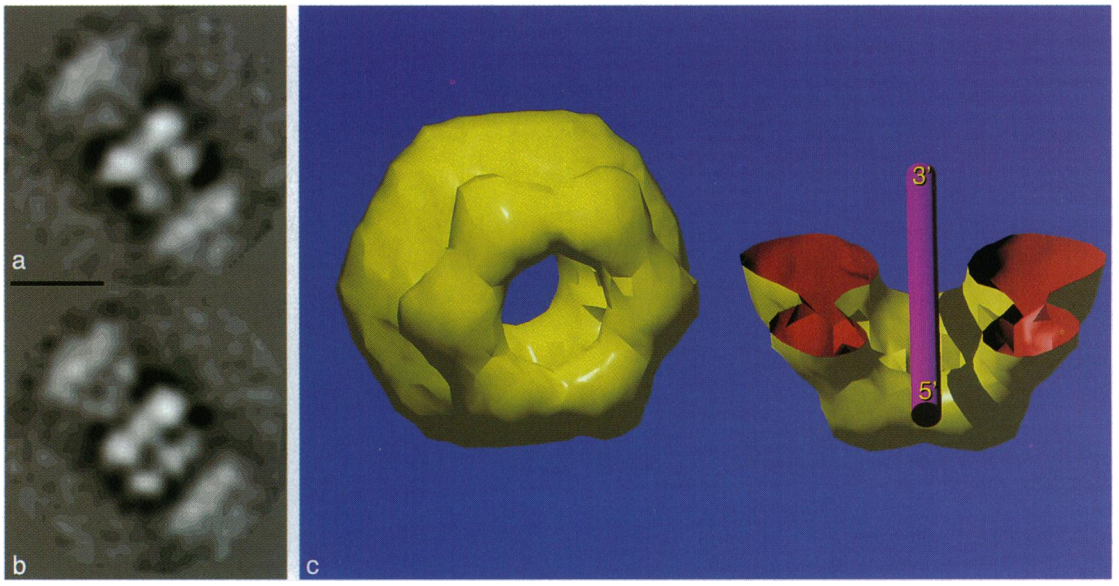

FIG. 5. A neural-net classification (9, 10) was applied to the 1000 side views of the 4B rings, and 469 images were found to be well aligned, while the remaining 531 images were found to be poorly aligned. The 469 images were then realigned, and the neural-net classification was then used to select 66 images (*a*) that formed one homogeneous group and 50 images (*b*) that formed a second homogeneous group. (Bar in *a* = 100 Å.) These two groups correspond to two characteristic projections of a hexameric ring, each related to the other by a 30° rotation about the axis of the DNA (19). Most of the remaining 353 images could be classified as intermediates between these two views. If it is assumed that the rings all have a random azimuthal orientation on the DNA, then the 66 images in *a* would contain an angular range of ±4.2°, while the 50 images in *b* would contain an angular range of ±3.2°. By imposing the sixfold symmetry, these two characteristic views generate 12 projections of the structure corresponding to a single-axis tilt series about the path of the DNA. This has been used to reconstruct the 4B hexamer (*c*) by using a weighted back-projection algorithm. The proof of the correctness of this reconstruction is that it generates a top-view projection nearly identical to that of Fig. 1*f*, even though that projection was not used in the reconstruction. A surface is shown on the left in *c*, based upon the known molecular mass of 4B (56 kDa) and assuming a partial specific volume for protein of 0.75 cm^3/g. Half of the structure has been removed on the right, and a rod indicates the path of the ssDNA. The rod has been labeled to show that the small end of the hexamer is at the 5′ end of the ssDNA.

DNA (28). Thus, the passage of DNA through the center of a hexameric ring is likely common to RuvB, gp4, and T antigen. Given the ubiquity of helicase proteins in both prokaryotic and eukaryotic DNA repair, recombination, replication, and transcription (24, 25, 29–32), a common three-dimensional organization of some of these proteins on DNA may suggest that specialized functions have evolved from a single ancestral structure.

We thank Gilene Oliveira and Kathy Kehret for their work in implementing the neural-net classification. This research was supported by National Institutes of Health Grant GM35269 (to E.H.E.) and American Cancer Society Grant NP 832 (to S.S.P.).

1. Kornberg, A. & Baker, T. A. (1992) *DNA Replication* (Freeman, San Francisco).
2. Lohman, T. M. (1992) *Mol. Microbiol.* **6,** 5–14.
3. Gorbalenya, A. E. & Koonin, E. V. (1993) *Curr. Opin. Struct. Biol.* **3,** 419–429.
4. Patel, S. S. & Hingorani, M. M. (1993) *J. Biol. Chem.* **268,** 10668–10675.
5. Patel, S. S., Hingorani, M. M. & Ng, W. M. (1994) *Biochemistry* **33,** 7857–7868.
6. Patel, S. S., Rosenberg, A. H., Studier, F. W. & Johnson, K. A. (1992) *J. Biol. Chem.* **267,** 15013–15021.
7. Penczek, P., Radermacher, M. & Frank, J. (1992) *Ultramicroscopy* **40,** 33–53.
8. Frank, J., Shimkin, B. & Dowse, H. (1981) *Ultramicroscopy* **6,** 343–358.
9. Kohonen, T. (1990) *Proc. IEEE* **78,** 1464–1480.
10. Marabini, R. & Carazo, J. M. (1994) *Biophys. J.* **66,** 1804–1814.
11. Bernstein, J. A. & Richardson, C. C. (1988) *Proc. Natl. Acad. Sci. USA* **85,** 396–400.
12. van Heel, M. & Frank, J. (1981) *Ultramicroscopy* **6,** 187–194.
13. Tabor, S. & Richardson, C. C. (1981) *Proc. Natl. Acad. Sci. USA* **78,** 205–209.
14. Matson, S. W., Tabor, S. & Richardson, C. C. (1983) *J. Biol. Chem.* **258,** 14017–14024.
15. Stasiak, A., Egelman, E. H. & Howard-Flanders, P. (1988) *J. Mol. Biol.* **202,** 659–662.
16. Hingorani, M. M. & Patel, S. S. (1993) *Biochemistry* **32,** 12478–12487.
17. Geiselmann, J., Wang, Y., Seifried, S. E. & von Hippel, P. H. (1993) *Proc. Natl. Acad. Sci. USA* **90,** 7754–7758.
18. Arnott, S. & Chandrasekaran, R. (1981) in *Biomolecular Stereodynamics I*, ed. Sarma, R. (Academic, New York), pp. 99–122.
19. Stasiak, A., Tsaneva, I. R., West, S. C., Benson, C. J. B., Yu, X. & Egelman, E. H. (1994) *Proc. Natl. Acad. Sci. USA* **91,** 7618–7622.
20. Notarnicola, S. M. & Richardson, C. C. (1993) *J. Biol. Chem.* **268,** 27198–27207.
21. West, S. C. (1994) *Cell* **76,** 9–15.
22. Lloyd, R. G. & Sharples, G. J. (1993) *Nucleic Acids Res.* **21,** 1719–1725.
23. Tsaneva, I. R., Muller, B. & West, S. C. (1993) *Proc. Natl. Acad. Sci. USA* **90,** 1315–1319.
24. Matson, S. W. & Kaiser-Rogers, K. A. (1990) *Annu. Rev. Biochem.* **59,** 289–329.
25. Lohman, T. M. (1993) *J. Biol. Chem.* **268,** 2269–2272.
26. Mastrangelo, I. A., Hough, P. V. C., Wall, J. S., Dobson, M., Dean, F. B. & Hurwitz, J. (1989) *Nature (London)* **338,** 658–662.
27. Wessel, R., Schweizer, J. & Stahl, H. (1992) *J. Virol.* **66,** 804–815.
28. Dean, F. B., Borowiec, J. A., Eki, T. & Hurwitz, J. (1992) *J. Biol. Chem.* **267,** 14129–14137.
29. Matson, S. W. (1991) *Prog. Nucleic Acids Res. Mol. Biol.* **40,** 289–326.
30. Deschavanne, P. J. & Harosh, I. (1993) *Mol. Microbiol.* **7,** 831–835.
31. Schaeffer, L., Roy, R., Humbert, S., Moncollin, V., Vermeulen, W., Hoeijmakers, J. H., Chambon, P. & Egly, J. M. (1993) *Science* **260,** 58–63.
32. Selby, C. P. & Sancar, A. (1993) *Science* **260,** 53–58.